THERMOMAGNETIC CONVECTION OF A MAGNETIC NANOFLUID INFLUENCED BY A MAGNETIC FIELD

Ali BOUHROUR [a*] ***and Djamel KALACHE*** [a]

[a] Theoretical and Applied Fluid Mechanics Laboratory. Faculty of Physics.
USTHB, B.P. 32, El-Alia, 16111, Algiers, Algeria
*<u>Corresponding author</u> <u>E-mail</u> : bouhrourali @ yahoo.fr

We present a numerical study of thermomagnetic convection in a differentially heated cavity. The magnetic nanofluid (ferrofluid) is subjected to a uniform magnetic gradient oriented at an angle ¨ with respect to the thermal gradient. The motivation for this work stems largely from a desire to extent preexisting works focused on horizontal and vertical orientations ¨=0°, 90°,180° and 270°. Our main goal is to get data on the flow and heat transfer for any orientation in the entire range 0J360°. The generalized problem lends itself to the investigation of orientations that give maximum heat transfer. It is found that (1) At a given magneto-gravitational coupling number N, orientations 0°, 90° and 270°, for which magnetization gradient is unstable, are not the optimum ones (2) For $0 \prec N \preccurlyeq 1$, heat transfer reaches a maximum between 270° and 360° (3) For $N \succ 1$, a second maximum occur between 0° and 90° owing to reverse flow phenomenon (4) At strong magnetic gradients, the two heat transfer peaks take the same value (5) Optimization parameter μ, reflecting the strongest magnetic effect, grows with N. Unlike the gravity, magnetic gradient may supply various strengths and spatial configurations, which makes thermomagnetic convection more controllable. Also, the magnetic mechanism is a viable alternative for the gravity one in microgravity, where thermogravitational convection ceases to be efficient.

Key words: *thermomagnetic convection, ferrofluid, maximum heat transfer, magnetization stratification, magnetic gradient, optimum orientation*

1. Introduction

Theory permits the possibility of liquid ferromagnetism, but the known ferromagnetic solids lose their strong magnetism and become paramagnetic above what is known as the Curie point, which is well below the melting point. The liquid ferromagnetism exists in the form of so-called magnetic nanofluids known also as ferrofluids (FFs). FFs are colloidal suspensions of mono-domain ferro-magnetic particles in a base liquid. The first stable FFs were produced in the mid-60s by the technique invented by Papell at NASA [1]. Nanoparticles are coated with a nonmagnetic surfactant layer which, together with the Brownian motion, inhibits their aggregation due to the ubiquitous magnetic and Van der Walls forces. FF synthesis is a veritable task [2,3]. Liquidity and strong magnetism explain the keen interest taken in FFs whose research field is multi-disciplinary. Chemists study their synthesis and physicists propose theories explaining their proprieties. Engineers study their applicability and use them in technical products. Biologists and physicians study their biomedical potential. FFs were first used as fuel in weightlessness [1]. Nowadays, they serve in a wide range of various areas such as sealing, damping and bio-medicine [3,4]. Unlike in classical magnetohydrodynamics (MHD), where Lorentz force can be nonzero even in a uniform magnetic field, the body force in ferrohydrodynamics (FHD) requires no currents but material magnetization and non-uniform field. At the basis of thermomagnetic convection (TMC) mechanism lays the interplay of a field with FF pyromagnetic properties. FFs are smart materials with promising potential for thermal engineering. They would have great advantages over ordinary liquids in devices where heat transfer is the limiting factor such as high-power transformers. The replacing the cooling oil of the transformer by a FF based on this oil can take advantage of the preexisting leakage magnetic fields to improve and maximize heat removal [5]. Besides the macroscopic applications, FFs may be a viable option to reinforce heat removal in challenging miniature systems where thermogravitational convection (TGC) cannot be harnessed [6]. Finlayson [7] was the first to propose a modification of the classical Bénard experiment to probe the way in which a uniform field affects the instability threshold in a FF. Schwab et *al*. [8] implemented the experiment suggested and confirmed the pioneer predictions [7]. Generalizations and extensions of the theoretical model [7] may be found in [9-16] to name a few. TMC in cavities has been studied both numerically and experimentally in magnetic fields created and controlled by various sources. Several authors studied the effect of a uniform field on heat transfer [17-23], while others assumed a nonuniform field [5,6,24-32]. This paper deals with TMC in differentially heated cavity placed in a uniform magnetic field gradient. Survey of works [24-28] has shown that studied are only the magnetic gradient horizontal and vertical orientations. To the best of our knowledge, no complete study was carried out on the magnetic gradient orientation effects. To remedy this lack of information, we assume a magnetic gradient arbitrarily oriented with respect to the thermal gradient and gravity.

2. Physical model

The working FF is confined in rectangular cavity made of non-magnetic materials to not distort the external non-uniform magnetic field $\vec{H}\mathrm{ex}$. The right hot and left cold walls of height L are kept at constant temperatures T_h and T_c, while the top and bottom walls of width W are isolated. The uniform magnetic gradient $\vec{\nabla}H\mathrm{ex}$ is oriented at an angle ¨ with respect to the thermal gradient $\vec{\nabla}T$ (fig. 1).

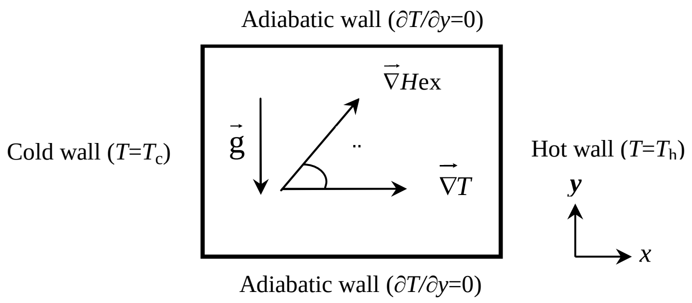

Figure.1. Physical system.

3. Ferrohydrodynamic model

The pioneer FHD model [33] treats the FF as non-conducting isotropic mono-component and mono-phase continuum with instantaneous magnetic relaxation, i.e., equilibrium magnetization is reached in times smaller than the characteristic convective time. This quasi-stationary macroscopic model holds for well-stabilized Newtonian FFs at low and moderate concentrations. Boussinesq approximation enables to write the coupled laminar thermomechanics equations describing the physical model as

$$\vec{\nabla}\,.\,\vec{\mathrm{v}}=0 \tag{1}$$

$$\rho_0\,(\frac{\partial}{\partial t}\;+\;\vec{\mathrm{v}}\,.\,\vec{\nabla})\;\vec{\mathrm{v}}\;=\;-\;\vec{\nabla}P\;+\;\rho\;\vec{\mathrm{g}}\;+\;\eta\;\nabla^2\;\vec{\mathrm{v}}\;+\;\mu_0(\vec{\mathrm{M}}\,.\,\vec{\nabla})\;\vec{\mathrm{H}} \tag{2}$$

$$\rho_0 C\,(\frac{\partial}{\partial t}\;+\;\vec{\mathrm{v}}\,.\,\vec{\nabla})T\;=\;\lambda\;\nabla^2 T\;-\;\mu_0\,T\,(\frac{\partial M}{\partial T})_{\mathrm{H}}\,(\frac{\partial}{\partial t}\;+\;\vec{\mathrm{v}}\,.\,\vec{\nabla})\,H \tag{3}$$

The last term in eq. (2) stand for the Kelvin magnetic force acting on the FF. The last term of eq. (3) reflects the FF temperature change due to the magnetocaloric effect which is associated both with the change in field intensity H with time and the FF motion along the magnetic field gradient lines. This adiabatic effect proves to be negligible far below the Curie temperature T_C and maximum near it.
With no conduction and displacement currents, Maxwell equations governing the total field $\vec{\mathrm{H}}$ are

$$\vec{\nabla}\,.\,(\vec{\mathrm{M}}\;+\;\vec{\mathrm{H}}\,)=\;0 \qquad\qquad \vec{\nabla}\;\times\;\vec{\mathrm{H}}\;=\;\vec{0} \tag{4 a – b}$$

FHD model [33] consider magnetically "soft" particles whose anisotropy energy $K_a V_f$ is much lower than their thermal energy $k_B T$, i.e., the magnetic moment is not frozen into the body particle so that the field does not affect the particle orientation. Thus, FF is free from magnetoviscous effect (MVE) [34]. With magnetization vector aligned with the field, the expression of the Kelvin body force becomes as

$$\vec{\mathrm{M}}=(M\,/\,\mathrm{H})\;\vec{\mathrm{H}} \qquad\qquad \vec{\mathrm{F}}=\mu_0 M\;\vec{\nabla}H \tag{5 a – b}$$

Nano-scaled sizes and low concentrations of particles weaken their magnetic interaction and thus their structurization in chains and clusters even in the absence of the field. Thus, Langevin's theory is adapted for mono-disperse identical particles to get the superparamagnetic magnetization law [35]

$$M=n_p m_p\;(\coth\xi\;-\;1/\xi) \tag{6}$$

where $\xi=\mu_0 m_P H\,(k_B T)^{-1}$ is the Langevin argument, $n_p=\varphi V_p^{-1}$ the particle concentration (φ is the solid volume fraction and V_p the particle hydrodynamic volume) and $m_P=M_f V_f$ the particle magnetic moment (M_f is the particle domain magnetization and V_f the particle volume ferromagnetic portion) .
In narrow ranges of H and T, the density and magnetization equations of state are linearized about the reference field H_r and the walls average temperature $T_0=(T_h+T_c)/2$

$$\rho=\rho_0\;+\;\rho_0\;\;\beta\;(T-T_0) \qquad\qquad M=M(H_r,T_0)\;+\;\chi\;\;(H-H_r)\;-\;K(T-T_0) \tag{7 a – b}$$

where $\chi=(\partial M/\partial H)_T$ is the magnetic susceptibility and $K=-(\partial M/\partial T)_H$ the pyromagnetic coefficient which, at magnetic saturation $M_{sat}=n_p m_p$ ($\xi\gg 1$) and weak magnetic fields ($\xi\ll 1$), is given by [36]

$$K=M_{sat}(\;\beta_m+\;\;\beta)\;\;\text{at}\;\;\xi\ll 1 \qquad K=(\xi M_{sat}\,/\,3)\,(1/T+2\;\beta_m+\;\;\beta)\;\;\text{at}\;\;\xi\ll 1 \tag{8 a – b}$$

where $\beta=-(1/\rho)\,(\partial\rho/\partial T)$ and $\beta_m=-(1/m_p)\,(\partial m_p/\partial T)$ which is very weak far below the Curie point.

In zero approximation, the field perturbation may be ignored, i.e., the field is assumed prescribed $(\vec{\mathrm{H}}\approx\vec{\mathrm{H}}\mathrm{ex})$ and Maxwell equations are mathematically isolated from others equations. Condition for zero approximation to be applied is $\nabla H\mathrm{ex}\gg\nabla H\mathrm{in}$ where $\nabla H\mathrm{in}\approx K\nabla T$ is the induced inner magnetic gradient by the non-isothermal FF. Thus, far below T_C, the steady dimensionless equations are cast in the form

$$\frac{\partial u}{\partial x}+\frac{\partial v}{\partial y}=0 \tag{9}$$

$$u\frac{\partial u}{\partial x}+v\frac{\partial u}{\partial y}=-\frac{\partial p}{\partial x}+\Pr\left(\frac{\partial^2 u}{\partial x^2}+\frac{\partial^2 u}{\partial y^2}\right)-\Pr(\mathrm{Rm}\cos\ddot{}\,\varphi \tag{10}$$

$$u\frac{\partial v}{\partial x}+v\frac{\partial v}{\partial y}=-\frac{\partial p}{\partial y}+\Pr\left(\frac{\partial^2 v}{\partial x^2}+\frac{\partial^2 v}{\partial y^2}\right)+\Pr(\mathrm{Rg}-\mathrm{Rm}\sin\ddot{}\,\varphi \tag{11}$$

$$u\frac{\partial n}{\partial x}+v\frac{\partial n}{\partial y}=\frac{\partial^2 n}{\partial x^2}+\frac{\partial^2 n}{\partial y^2} \tag{12}$$

Dimensionless temperature is n=(T–T_0)/T_h−T_c. Boundary conditions consist of no-slip on all walls (u=v=0), zero heat flux across the top and bottom walls (∂n/∂y=0) and isothermal right and left walls (n=±0.5). Control parameters are: the aspect ratio Ar=L/W, Prandtl number Pr=C¦/ª, gravitational and magnetic Rayleigh numbers Rg= ∘$g\nabla TW^4$/¬a and Rm=«$_0K\nabla H\nabla TW^4/a$¦. Magnetogravitational coupling number N=Rm/Rg=«$_0K\nabla H$/°$_0$ ∘g is the ratio of thermomagnetic force (TMF) to thermogravitational one (TGF). Besides being dependent on the field and T-distribution, TMC is affected by the pyromagnetic coefficient. Thus, to strengthening it one can use either solids with higher K or higher £. So, thermo-sensitive FFs, whose magnetization strongly depend on temperature, are needed. Only near T_C a change in T cause a high change in M. Usual ferromagnets have high T_C, e.g. 1331[°C] for cobalt. So, considering the base liquid boiling point, FFs with T_C close to the devices operating range are needed. Table 1 show high K and low T_C for Mn-Zn and Fe-Zn ferrites, and various FFs used in different studies.

Table 1. Pyromagnetic coefficient of thermo-sensitive FFs and various FFs used in different studies on TMC.

Reference	*Carrier liquid*	*Magnetic material*	£ (%)	T_C [°C]	K [A m^{-1}K^{-1}]
Parekh *et al.* [37]	Diester	$Mn_{0.5}Zn_{0.5}$–Fe_2O_4	8.91	67	5125
	Diester	$Fe_{0.5}Zn_{0.5}$–Fe_2O_4	4.94	91	3125
	Diester	$Fe_{0.3}Zn_{0.7}$–Fe_2O_4	6.99	74	2128
Li *et al.* [38]	Kerosene	Mn Zn–Fe_2O_4	4.50	80	1050
Sustov [39]	Kerosene	Fe_3O_4	–	–	100
Engler *et al.* [40]	Synthetic ester	Fe_3O_4	6.30	–	35.3
Tangthieng *et al.* and Jue [5,30]	Hydrocarbon oil	Fe_3O_4	1.60	–	30
Schwab *et al.* and Stiles and Kagan [8,9]	Hydrocarbon	–	–	–	27.3
Sawada *et al.* [26]	Water	Fe_3O_4	–	–	24

To estimate the heat flux at the hot wall, the local and mean Nusselt numbers are calculated as

$$\mathrm{Nu}=\frac{h\,W}{a}=\left.\frac{\partial n}{\partial x}\right)_{x=1} \qquad \overline{\mathrm{Nu}}=\frac{\int_0^{Ar}\mathrm{Nu}(y)\,dy}{Ar} \tag{13}$$

4. Association phenomena and transport properties of FFs

A typical FF contains on the order of 10^{23} particles per cubic meter, and collisions between them are frequent. Particles clustering may be regarded as a step in the direction of sedimentation which may destroy the FF. In strong fields, particles tend to form chains parallel to the field with a mean particles number n_∞=[1– 0.66£¥$^{-2}$e$^{2\gamma}$]$^{-1}$ [41] (¥ is the coupling parameter). Like any fluid, hydro-thermal processes in FFs are affected by changes in its thermophysical properties. The highly stable Newtonian i-butanol based FF show no MVE while the methyl-ethyl-ketone based FF show a strongly non-Newtonian behavior owing to a significant increase of its effective viscosity ¦ caused by aggregation initiated by an incomplete surfactant covering of particles [3]. Stability analysis and experiment show that the MVE delay the TMC onset [15,40]. Higher TMC threshold in sample with coarser particles is due to chain-like structures causing a strong MVE reinforcing the stabilizing viscous forces which in turn hinder TMC [40]. In the theoretical model describing the MVE [42], which agree with experiment [43], increment of ¦ for the Co-toluene FF in a field parallel to the flow is higher than that for a normal field. However, in [44], MVE for a normal field is stronger than the very weak one in a parallel field. These data agree well with experimental data for the Fe-water FF [45]. Non-magnetic nanofluids exhibit effective thermal conductivity ª higher than that of carrier liquid, which is benefit for thermal applications. In [46] a new cooling system is proposed where the use of the Al_2-water nanofluid may limit thermal stresses in wind turbines. Some works focused on FFs thanks to their special properties. It is found that for a kerosene-base FF, ª grows with the strength of a field parallel to heat flux while a normal field has no effect [47]. The measured data for the Fe-water FF [45] agree with data of [47]. High increase of ª in a parallel field is also found for Fe_3O_4 in kerosene, hexadecane or oil [48,49]. In [45, 48-50], it is claimed that aggregates and their aspect ratio plays a vital role in the grows of anisotropic ª. In [51], ª grows with H for the parallel alignment while for the normal case, it has an inverse relationship to H. Experiment fit well with prediction [52]. As outlined in [53], besides the apparent paradox about the field direction effect on FF thermal and rheological properties, these studies were conducted in the stagnant state. Thus, the question is can aggregates be build in magnetic fields and affect properties of flowing FFs ?

5. Numerical method and solution procedure

Finite volumes method [54] is used to discretize eqs. (9–12). Pressure-velocity coupling is handled by the SIMPLER algorithm. Under-relaxed algebraic equations are solved with a tri-diagonal matrix algorithm line-by-line solver. A residual shows how perfectly these equations are satisfied. Numerical tool was checked for accuracy against benchmark data [55] for TGC of air (Pr=0.71) and Ar=1. We get $\overline{\mathrm{Nu}}$ = 1.118 *vs* 1.118, 2.244 *vs* 2.243, 4.535 *vs* 4.519 and 8.866 *vs* 8.800 for Rg=10^3, 10^4, 10^5 and 10^6. Good accord between both data highlights adequacy of numerical tool. For TMC, grid dependency tests are performed at Rg=10^4, Pr=7 and Ar=1 on the grids 61×61 and 231×231 for four magnetic gradient orientations: ¨=0°, 45°, 225° and 315° with two values of N tested for each ¨. The $\overline{\mathrm{Nu}}$ and deviations based on the finest grid are listed in tab.2. It is seen that data obtained with both grids are very close with a good relative error. Thus, as for pure TGC, the grid 61×61 is chosen as a trade-off between calculus time and accuracy for all computations, except for higher Ar and high N where it is refined.

Table 2. Grid-dependence of TMC data at various magnetic gradient orientations. Rg=10^4. Pr=7. Ar=1.

¨ (°)	N	Grid size	$\overline{\mathrm{Nu}}$	Deviation (%)
0 (45) (225) (315)	1	61×61	2.823 (2.241) (2.244) (3.034)	–0.5 (–1.3) (0.6) (–0.1)
		231×231	2.828 (2.254) (2.238) (3.035)	–
	25	61×61	4.869 (6.257) (2.596) (6.431)	–3.4 (4.3) (5.3) (4.8)
		231×231	4.903 (6.214) (2.543) (6.383)	–

6. Results and discussion

6.1. Horizontal and vertical orientations ¨ = 0°, 180°, 90° and 270° of the magnetic gradient

Berkovsky *et al*. [24] conducted experimental and numerical studies of TMC in a layer (Ar=27) of kerosene-based FF (Pr=36) prepared by magnetite (Fe_3O_4) particles dispersion (£=1.2%) with acid oleic admixed as a stabilizer agent. The FFù is placed in a horizontal magnetic gradient ∇H=3.1·10^5 [A m^{-2}]. Computations showed that at Ar≻5, increasing Ar result in slight decrease of $\overline{\mathrm{Nu}}$, e.g. at Rm=10^6 and Rg=3.6·10^5, $\overline{\mathrm{Nu}}$ for Ar=10 exceeds the measured one by less than 10%. Possibility of extrapolation suggested them to study numerically the magnetic effect. Qualitative accord is seen between data [24] (fig.2) and our results (fig.3) for Ar=5. When $\vec{\nabla} H$ and $\vec{\nabla} T$ are parallel (¨ =0°), the magnetization gradient is unstable ($\vec{\nabla} M \uparrow\downarrow \vec{\nabla} H \downarrow\downarrow \vec{\nabla} T$). The cold layers (higher M) are sucked into zones of higher H displacing the hot layers (lower M). Thus, TMC enhance TGC. Horizontal lines of curves 1-2-3 indicate a weak magnetic effect as compared to the gravity one. TGC enhancement takes place when TMF is competitive to TGF (Rmù Rg). Higher the Rm more will be TMF leading to higher $\overline{\mathrm{Nu}}$. At strong ∇H, the three curves overlap each other indicating a same $\overline{\mathrm{Nu}}$ due to a weak gravity effect, e.g. at Rg (or Ra) =10^3, is compensated by a strong magnetic effect, e.g. N=5·10^3 at Rm=5·10^6, as compared to cases Rg=10^4 (N=5·10^2) and Rg=10^5 (N=50). If $\vec{\nabla} H$ and $\vec{\nabla} T$ are adverse (¨ =180°), the magnetization gradient is stable ($\vec{\nabla} M \uparrow\uparrow \vec{\nabla} H \uparrow\downarrow \vec{\nabla} T$), i.e., TMC works against TGC. Horizontal lines of curves 1'-2'-3' reflect a weak damping effect which becomes significant at Rmù Rg. Then, $\overline{\mathrm{Nu}}$ reduce with Rm until unity. Cold layers are so fixed by the TMF so that heat transfer is by conduction ($\overline{\mathrm{Nu}}=1$). The required Rm to suppress the flow grows with Rg. TMC is not associated with gravity. Thus, FF greatest interest is when it is used in microgravity conditions, where cooling by TGC ceases to be efficient (e.g. orbital stations). $\overline{\mathrm{Nu}}$ *vs* Rm is plotted in fig.4 for ¨ =0° and Rg=0. Horizontal line for pure conduction ($\overline{\mathrm{Nu}}=1$)

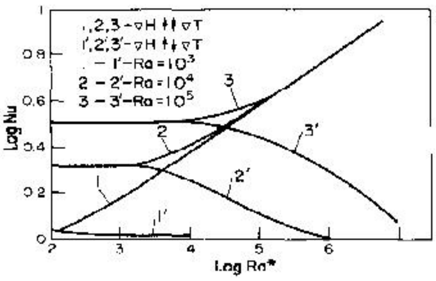

Figure. 2. An effect of gradient magnetic field on heat transfer for *Ar*=5 (Berkovsky et *al*. [24]).

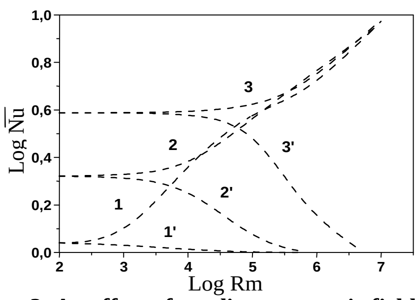

Figure.3. An effect of gradient magnetic field on heat transfer for *Ar*=5 (Present work).

breaks up when TMC comes into play as soon as TMF will overcome the stabilizing effects of viscosity and thermal diffusion. Beyond the TMC threshold (~2700) (fig.4), $\overline{\mathrm{Nu}}$ grows with Rm. We can speak of magnetic Rayleigh-Bénard system with horizontal magnetic gravity gm_X=+Ng. In elegant experiment [56], TMC is studied in microgravity using sounding rockets and at the drop tower.

When $\vec{\nabla} H$ augmentsgravity, the magnetization gradient is unstable (¨ =270° $\vec{\nabla} H \downarrow\downarrow \vec{g} \perp \vec{\nabla} M \uparrow\downarrow \vec{\nabla} T$). Thus, TMF acts in the same direction than TGF with an apparent gravity ga=g+gm_y where gm$_y$=+Ng is a pseudo vertical magnetic gravity). Horizontal line in fig.5 implies a dominant role for TGC. At N≻0.1, the magnetic effect grows with N. When $\vec{\nabla} H$ opposes gravity, $\vec{\nabla} M$ is also unstable (¨ =90° $\vec{\nabla} H \uparrow\downarrow \vec{g}$), but TMF opposes TGF. At N≺1, TGF is dominant since gm$_y$=–Ng (ga≻0). Horizontal line reflects a weak damping magnetic effect which start to grow beyond N=0.1. At N=1, TMF and TGF are ideally turned off (ga=0, $\overline{\mathrm{Nu}}$=1) as shown by vertical isotherms in fig.6. For N≻1, TMF is strong enough to reverse the flow (ga≺0), i.e., the warm FF spreads downward and $\overline{\mathrm{Nu}}$ grows as |ga| grows with N. Reverse flow is illustrated by the isotherms traced for N=0.9, which are upside down compared to those of N=1.1. The velocity vector field evidences clarify this phenomenon. Flow is counter-clockwise at N=0.9 and clock-wise at N=1.1. Figure 5 shows a symmetry about the line N=1, where $\overline{\mathrm{Nu}}$ is the same for 0≼N$_1$≺1

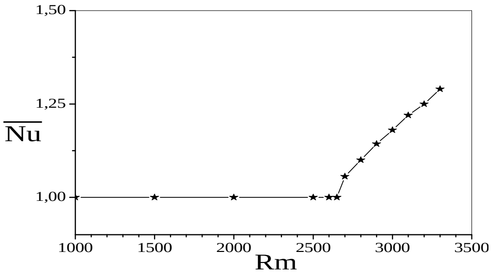

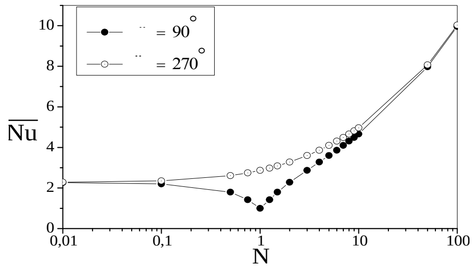

Figure. 4. Ferroconvective instability in microgravity ¨=0° ($\vec{\nabla}$e ë í $\vec{\nabla}$q) *Ar*=1. Pr=36. Rg= 0.

Figure. 5. Heat transfer versus magnetic gradient strength ¨=90° ($\vec{\nabla}H$ ë í $\vec{g}$) and ¨=270° ($\vec{\nabla}H$ í í $\vec{g}$) *Ar*=1. Pr=7. Rg=10^4.

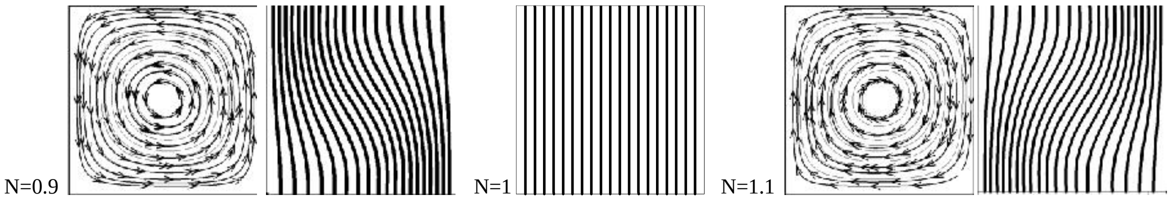

Figure. 6. Velocity vector field and temperature iso-lines illustrating the reverse flow for *φ*=90°. *Ar*=1. Pr=*7*. Rg=10^4.

and$1 \prec N_2 \preccurlyeq 2$ with $N_1+N_2=2$. This occurs because the FF feels the same net force, i.e., $ga(N_1)=|ga(N_2)|$.This symmetry has been observed in [25] for ga=9.8 [ms^{-2}] (N_1=0) and ga=−10 [ms^{-2}] ($N_2\approx2$ corresponding to $\nabla H=5.37\cdot10^5$ [A m^{-2}]). Also, $\overline{Nu}$ for ¨=90° at $N_1 \succ 2$ equals $\overline{Nu}$ for ¨ =270° at N_2, such as $N_1-N_2=2$, because the FF feels the same net force ($|ga\ (N_1)|=ga\ (N_2)$). At $N \succ 1$, the disparity between $\overline{Nu}$ at ¨=90° and $\overline{Nu}$ at ¨=270° reduces until zero at high N where they overlap each other due to a weak gravity effect. Table 3 displays a comparison with prediction [28] and experiment [26] where three FFs are tested, W-40 (Fe_3O_4-water), TS-40W (Mn-Zn-water) and HC-50 (kerosene-base). Comparison is for W-40 since more data are given about its properties (Rg=37560, Pr=44.3). Excellent accord between the 2D data is evident. For pure TGC (N=0), where the FF behaves as the base liquid since M=0, prediction is in poor accord with experiment while 2D data are adequate for low Rg laminar

Table 3. Comparison with experiment [26] and simulation [28] for ¨=90° and ¨=270°. *Ar* =1. Rg=37560. Pr=44.3.

¨ (°)	$\nabla H\times10^5$ [A m^{-2}]	$ga\lfloor g$	N	2D [28]	2D (Present work)	3D [28]	Experiment [26]
–	0	1	0	3.50	3.49	3.37	5.0
270	1.6	2.1	1.1	4.41	4.41	4.38	5.1
	4.5	4.0	3.0	5.34	5.34	5.47	5.3
	8.8	6.9	5..9	6.29	6.29	6.59	5.9
90	1.6	−0.1	1.1	1.63	1.62	1.47	2.1
	4.5	−2.0	3.0	4.34	4.34	4.30	3.9
	8.8	−4 9	5.9	5.69	5.69	5.87	5.6

flow and the literature values average 3.75 [28]. For instance, Lankhorst [57] captured data for both water (Pr=8.11) and air in one correlation: $\overline{Nu}=[0.31\ Pr^{0.035}\ Rg^{0.25}]^{\ a}$ (a=1–15.62 $Rg^{-0.431}$) for $600 \prec Rg \preccurlyeq 10^6$. The power 0.035 reflects the Pr’s weak effect, also found here and in [28]. His 2D and 3D numerical data differ by only 0.04%. Also, 2D data agree well with those of [55]. His correlation gives $\overline{Nu}$=2.202 *vs* 2.243 , 4.526 *vs* 4.519 and 8.834 *vs* 8.800 at Rg=10^4, 10^5 and 10^6. For Rg=37560 and Pr=44.3, it gives $\overline{Nu}$=3.77. Excellent fit is achieved between simulation and his own experiments. Moreover, his data agree well with measurements of other investigators. To compare with experiment, it is required to known many of W-40 properties accurately. Density and kinematic viscosity ¬ are given in [26]. As the thermal expansion coefficient, that of water is adopted: $_\rho$=$2.6\cdot10^{-4}$ [K^{-1}] [58]. Unfortunately, as pointed out [58], because the FF is a mixture with complex physicochemical properties, it was very difficult to obtain the exact values of specific heat C and ª, which are estimated from literature:

C=3.0·10^3 [J Kg^{-1}K^{-1}] is computed using C_w and C_f of water and Fe_3O_4 found in [59] and particles diameter given in [60] is used to get ª using a formula provided in [61] for Co or Fe in toluene or hydrocarbon oil. Both ª$_w$ and ª$_f$ are found in [62]. However, as mentioned above, various FFs may have various models for ª. Besides, both FFs used in [26, 58] have the same °=1.4·10^3 [Kg m^{-3}] and different ¬ (28.5·10^{-6} [m^2 s^{-1}] [26] and 8.7·10^{-6} [m^2 s^{-1}] [58]). Note that Pr=13.53 in [58], i.e., ¦=39.9 [Kg m^{-1}s^{-1}] in [26] is 3.28 times greater than ¦=12.8 [Kg m^{-1}s^{-1}] in [58]. Thus, both samples have different £. Since FF properties are affected by £, why both samples have the same C and ª but different ¦ ? Besides, the surfactant layer is considered in estimating ª and ignored in that of C. Unfortunately, there is no companion numerical study for experiment in [26] for complete comparison. So, it is probably unreasonable to expect a precise comparison of data. Relatively good accord is found at ¨=90°. Note that the reverse flow (ga≺0) for TS-40W occurs at smaller ∇H due to its higher K [26]. At ¨=270°, computation agree with experiment for ga/g=4 but not for ga/g=2.1 and 6.9. There is another unexplained result. The previous symmetry is found for ¨=90° (ga/g=–2) and ¨=270° (ga/g =2.1) (N_1–N_2≈**2** and **7**% of difference) while measured data differ by 120%.

6.2. Generalized problem

Simulations are for a water-based FF (Pr=7), Ar=1 and Rg=10^4. The angle ¨ is varied from 0° to 360° in steps of 5°. Generalized apparent gravity is written as $\vec{G}=\vec{g}+Ng\,\vec{e}$ ($\vec{e}$ is unit vector in direction of $\vec{\nabla}H$). Horizontal and vertical gravities are gm_x=+Ncos¨ g and ga=g+gm_y where gm_y= –Nsin¨ g. At N≼1, vertical TMF never exceed TGF (ga ∝0), i.e. the flow cannot be reversed as shown by the velocity vector field for N=1 in fig.7. Flow is that of one counter-clockwise rotating cell in the entire domain 0–360°. The $\vec{\nabla}H$ turn causes the cell turning due to change in TMF components. As is known, heat

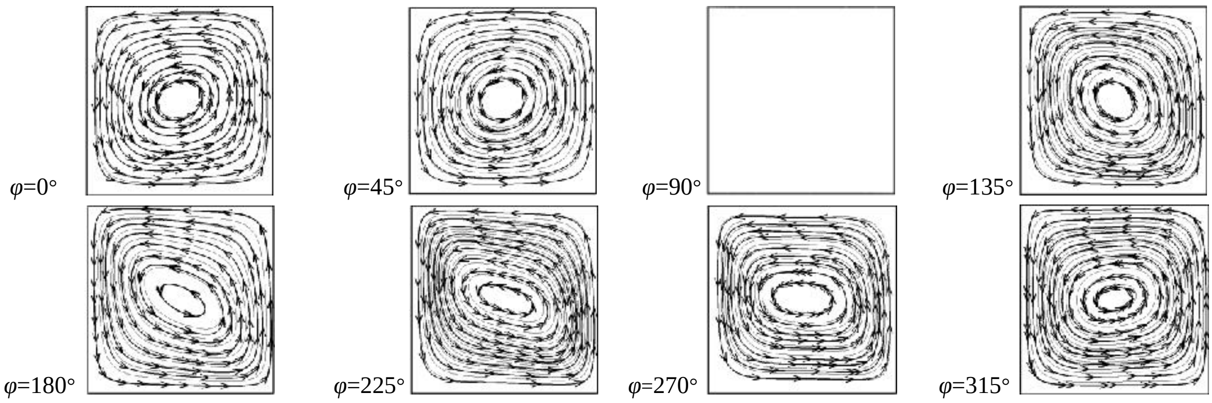

Figure. 7. Velocity vector field (streamlines) at various magnetic gradient orientations. *Ar*=1. Rg=10^4. Rm=10^4 (N=1).

transfer depends on the flow structure. Thus, change in $\vec{\nabla}H$ direction may cause change in heat flux across the cavity. Figure.8a depicts $\overline{\mathrm{Nu}}$ vs ¨. In 0–90°, TMC enhance partly TGC (gm_x≻0 $\vec{\nabla}H_x \downarrow\downarrow \vec{\nabla}T$ gm_y≺0 $\vec{\nabla}H_y \uparrow\downarrow \vec{g}$). The decrease of $\vec{\nabla}H_x$ with ¨ causes a decrease of gm_x while ga reduces ($|gm_y|$ grows) with growing $\vec{\nabla}H_y$. The resulting flow intensity decrease leads to lower $\overline{\mathrm{Nu}}$. In 90–180°, where TMC opposes totally TGC (gm_x≺0 $\vec{\nabla}H_x \uparrow\downarrow \vec{\nabla}T$ gm_y≺0 $\vec{\nabla}H_y \uparrow\downarrow \vec{g}$), $\overline{\mathrm{Nu}}$ declines with ¨ and passes through a minimum at $\varphi_{\min}$ reflecting the strongest damping magnetic effect. This trend is ascribable to its dependence upon the opposite effects of increasing ga (decreasing $|gm_y|$) and $|gm_x|$. In 90°–$\varphi_{\min}$, the drop of $\overline{\mathrm{Nu}}$ with growing $|gm_x|$ overcomes its increase with growing ga. The opposite occurs between $\varphi_{\min}$ and 180°. At N=1, the minimum is reached before reaching ¨=90° where the flow pattern die out

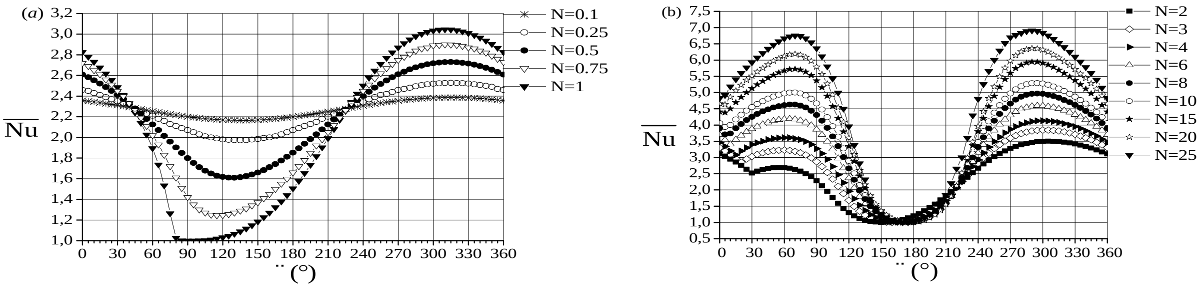

Figure. 8. Dependence of heat transfer rate on magnetic gradient orientation. ***Ar*=1. Pr=*7.* Rg=10^4 (a) N≼1 (b) N≻1.**

(fig.7) due a to mutual neutralization of TMF and TGF (G=0). This state persist from 80° until 115° (fig.8a) due to the weak apparent gravity in 80–90° (gm_x=+0.17g and ga=+0.02g at φ=80°) while the net vertical driving force is not strong enough to overcome the horizontal TMF resistant effect in 90–115° (gm_x=–0.42g and ga=+0.09g for φ=115°). At φ ≻115°, this effect is overwhelmed and convection sets in (gm_x=–0.5g and ga=+0.13g at φ=120°). As in 0–90°, TMC is partly cooperating in 180–270° but $\vec{\nabla}H$ components are inverted (gm_x≺0 $\vec{\nabla}H_x$↑↓$\vec{\nabla}T$ gm_y≻0 $\vec{\nabla}H_y$↓↓$\vec{g}$). As φ grows, $\vec{\nabla}H_x$ reduce while $\vec{\nabla}H_y$ increase. Hence, thflow resistance decrease with reducing $|gm_x|$ and increase of its intensity with growing ga (growing gm_y) leads to higher $\overline{Nu}$. In 270–360°, TMC enhance totally TGC (gm_x≻0 $\vec{\nabla}H_x$↓↓ $\vec{\nabla}T$ gm_y≻0 $\vec{\nabla}H_y$↓↓$\vec{g}$). The $\overline{Nu}$ grows with φ and passes through a maximum $\overline{Nu}_{max}$ at φ_{opt}. Between 270° and φ_{opt}, the increase of $\overline{Nu}$ as a result of increasing gm_x prevails on its decrease as a result of reducing ga (reducing gm_y). The opposite is true between φ_{opt} and 360°. At N≻1, the vertical TMF equilibrates TGF at φ_e given by N$sin\varphi_e$=1 (ga=0). At φ ≻φ_e, this force is strong enough to reverse the

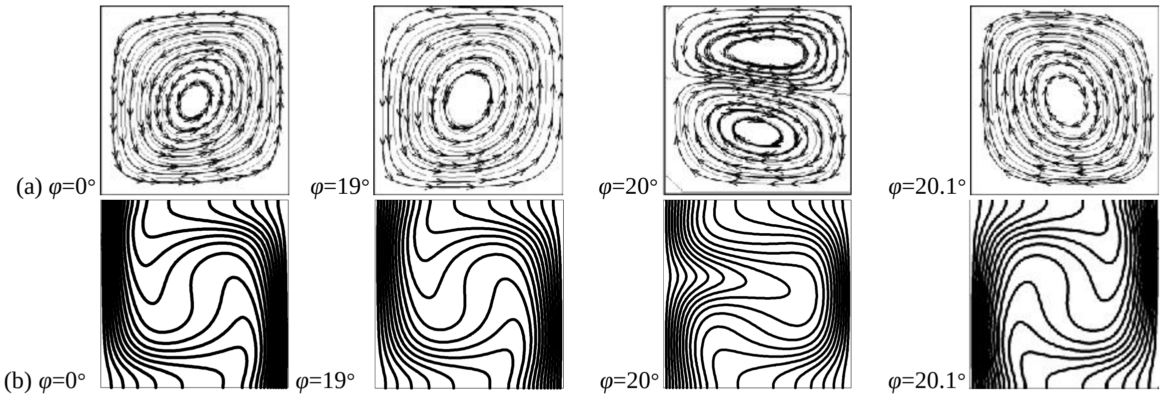

Figure. 9. (a) Velocity vector field and (b) isotherms at various magnetic gradient orientations. Rm=3.10^4 (N=3).

flow as shown for N=3 (fig. 9). In 0–19°, uni-cellular flow is rotating counter-clockwise. At 20°, one cell mode vanishes and two-cell mode rise. This case is similar to that studied for φ=0° in microgravity, i.e., Rm_x=2.82·10^4 lies at a supercritical state. Physically, heat supplied by the hot wall is transported towards the cold one thanks to the horizontal TMF (gm_x=+2.82g). Flow and thermal fields are exactly those for pure TGC (N=0) at Rg=2.82·10^4 in Rayleigh-Bénard system rotated of 90°. Beyond φ_e (φ=20.1°), two cells vanishes and one clockwise cell rise. To locate φ_e in the range 2≼N≼25, an increment Δφ=0.1° is used. A mean difference of 0.64° between computation and theory may be considered as sufficiently accurate since the lowest value is 2.29° for N=25. In 0–φ_e, TGF is dominant (ga≻0). The decrease of both gm_x and ga (grow of $|gm_y|$) with φ leads to weaker flow intensity causing the $\overline{Nu}$ drop until reaching a first minimum at φ_e (fig.8b). Beyond φ_e, the flow is reversed (ga≺0). In φ_e–90°, $\overline{Nu}$ grows to reach a first peak $\overline{Nu}_{1max}$ at φ_{1opt} after which it reduces. In φ_e–φ_{1opt}, the grow of

$\overline{\mathrm{Nu}}$ with growing $|ga|$ (growing $|gm_y|$) overcomes its reduce with reducing gm_x. The opposite is true in ¨$_{1opt}$–90°. For 90°≼¨≺180°–¨$_e$, vertical TMF is still dominant (ga≺0). Reducing $|ga|$ (reducing $|gm_y|$) and growing $|gm_x|$ with ¨ leads to lower $\overline{\mathrm{Nu}}$ and ¨=180°– φ_e yield a second minimum $\overline{\mathrm{Nu}}$=1 (ga=0 , gm_x≺0). Except at N=2, the flow is conduction dominated in 180°–¨$_e$≺¨≼180° due to a strong horizontal TMF (gm_x=–3g at N=3 and ¨=180°). As for N≼1, a second peak $\overline{\mathrm{Nu}}_{2max}$ is reached at ¨$_{2opt}$ in 270–360°.

6.3. Heat transfer optimization

Orientations ¨=0°, 90° and 270°are not the optimum ones (figs. 8a-b), owing to the TMF components effect on FF motion. For 0.1≺N≼1, the heat transfer peak occurs in 310–315°, while for 1≺N≼25, the two peaks are reached in 55–70° and 290–305°. The two optimum orientations moves towards ¨=90° and ¨=270° without reaching them. This also holds for higher N since varying N from 25 to10^5 results in small change in ¨$_{1opt}$ and ¨$_{2opt}$. For N∝85, the two peaks occurs at 75° and 285°, and take the same value due both to the week gravity effect (ga≈gm_y) and the symmetry of 75° and 285° about x-direction, i.e., TMF has the same strength (gm_x=+0.26Ng , gm_y=+0.96Ng at ¨=75° and gm_y=–0.96Ng at ¨=285°). The most remarkable magnetic action on heat transfer is described by a useful quantity: the scaled $\overline{\mathrm{Nu}}_{max}$

$$\mu = \frac{\overline{\mathrm{Nu}}_{max}}{\overline{\mathrm{Nu}}_0} \qquad (14)$$

Evaluating the optimization parameter μ at a given N require the $\overline{\mathrm{Nu}}_0$ for pure TGC at the same Rg. Here, $\overline{\mathrm{Nu}}_0$ =2.27 for Rg=10^4. It is seen that μ is always greater than one, indicating an enhancement of TGC (fig.10), e.g. at N=25 the maximum heat flux is three times higher than that for pure TGC (μ=3).

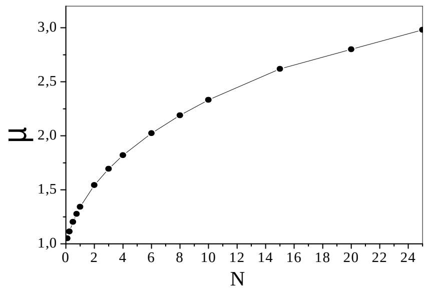

Figure. 10. TGC maximum enhancement versus magnetic gradient intensity. *Ar*=1. Pr=*7.* Rg=10^4.

7. Summary and conclusions

We performed a numerical study of TMC in a vertical cavity. The hydro-thermal processes are found to be sensitive to the magnetic gradient strength and its synergic orientation with thermal gradient and gravity. Orientations 0°, 90°and 270°, for which magnetization stratification is unstable, are not the optimum ones. At weak magnetic gradients, the heat transfer peak occurs in 270-360°. At higher values, a second peak occurs in 0-90° due to reverse flow phenomenon induced when vertical TMF becomes dominant over TGF. At strong magnetic gradients, the two peaks take the same value. FFs are controllable cooling agents in which flow and heat transfer may be adjusted by a proper choice of a magnetic gradient which, unlike gravity which is almost similar everywhere, may supply various strengths and orientations. In weightlessness or microgravity environment, where TGC is prohibited or not efficient, TMC mechanism remains the only one to ensure heat transport. Also, TMC requires both thermal and magnetic interactions with the surrounding. This makes using FFs as heat carrier a good option to improve the cooling system efficiency of devices which already have strong magnetic fields.

Nomenclature

- *a* – thermal diffusivity (=ª /° *C*), [$m^2 s^{-1}$]
- *Ar* – cavity aspect ratio (=*L*/*W*), [–]
- *C* – specific heat at constant pressure, [$J\ kg^{-1} K^{-1}$]
- *g* – normal gravity acceleration, [$m\ s^{-2}$]
- *ga* – apparent vertical gravity (= $g+gm_y$), [$m\ s^{-2}$]
- gm_x – apparent horizontal magnetic gravity, [$m\ s^{-2}$]
- gm_y – apparent vertical magnetic gravity, [ms^{-2}]
- *h* – local heat transfer coefficient, [$W\ m^{-2} K^{-1}$]
- *H* – magnetic field strength, [$A\ m^{-1}$
- *K* – pyromagnetic coefficient, [$A\ m^{-1}K^{-1}$]
- K_a – magnetocrystalline anisotropy constant, [$J\ m^{-3}$]
- k_B – Boltzman's constant, (= $1.3807{\cdot}10^{-23}$ [$J\ K^{-1}$])
- m_p – nanoparticules magnetic moment, [Am^{-2}]
- *M* – ferrofluid magnetization, [$A\ m^{-1}$]
- M_f – solid saturation spontaneous magnetization, [$A\ m^{-1}$]
- n_P – number of nanoparticles per unit volume, [m^{-3}]
- N – coupling number (=Rm/Rg =«$_0K\nabla H$/° $_\rho g$), [–]
- Nu – local Nusselt number (=*hW*/ª), [–]
- Pr – Prandtl number (=¦*C*/ª), [–]
- Rg – gravitational Rayleigh number (= $_\rho g\nabla TW^4$/¬*a*), [–]
- Rm – magnetic Rayleigh number (=«$_0K\nabla H\nabla TW^4$/¦*a*), [–]
- V_f – particle volume ferromagnetic portion, [m^3]
- V_p – particle hydrodynamic volume, [m^3]

Greek symbols

- ◦ – thermal expansion coefficient, [K^{-1}]
- $_m$ – magnetic moment thermal coefficient, [K^1]
- ¥ – coupling parameter, (=«$_0M_f^2V_f(24k_BT)^{-1}$), [–]
- £ – magnetic phase volume fraction, [–]
- ¶ – Langevin argument, (=«$_0\ m_pH\ (k_BT)^{-1}$),[–]
- ¦ – dynamic viscosity, [$kg\ m^{-1}s^{-1}$]
- n – dimensionless temperature, [–]
- ª – thermal conductivity, [$W\ m^{-1}\ K^{-1}$]
- ¬ – kinematic viscosity, [m^2s^{-1}]
- μ_0 – permeability of vacuum, (=$1.257{\cdot}10^{-6}$ [$N\ A^{-2}$])
- ° – density, [$kg\ m^{-3}$]
- ¨ – orientation angle of magnetic gradient, [°]
- i – magnetic susceptibility, [–]
- µ – heat transfer optimization parameter, [–]

Subscripts, abbreviations and acronyms

- C- e- f – Curie - equilibrium - ferromagnetic
- p- max-opt – particle - maximum- optimum
- TMC (F) – thermomagnetic convection (force)
- TGC (F) – thermogravity convection (force)
- FF-FHD – ferrofluid - ferrohydrodynamic-
- MVE – magnetoviscous effect

Acknowledgments We would like thanks Pr. T. Sawada (Keio University) who provided us his original experimental paper.

References

[1] Papell, S.S., Low Viscosity Magnetic Fluid obtained by the Colloidal Suspension of Magnetic Particles, U.S. patent 3215572, 1965

[2] Berger, P., *et al*., Preparation and Properties of an Aqueous Ferrofluid, *J. Chem. Educ., 76* (1999), 7, pp. 943-948

[3] Vekas, L., Magnetic Nanofluids Properties and Some Applications, *Rom. J. Phys*., *49* (2004), 9-10, pp. 707-721

[4] Raj, K., Moskowitz, B., Commercial Applications of Ferrofluids, *J. Magn. Magn. Mater*., *85* (1990), pp. 233-245

[5] Tangthieng , C. , *et al*., Heat Transfer Enhancement in Ferrofluids Subjected to Steady Magnetic Fields, *J. Magn. Magn. Mater., 201* (1999), pp. 252-255

[6] Mukhopadhyay, A., *et al*., A Scaling Analysis to Characterize Thermomagnetic Convection, *Int. J. Heat Mass Transfer, 48* (2005), pp. 3485-3492

[7] Finlayson, B.A., Convective Instability of Ferromagnetic Fluids, *J. Fluid Mech*., *40* (1970), 4, pp. 753-757

[8] Schwab, L., *et al*., Magnetic Bénard Convection, *J. Magn. Magn. Mater*., *39* (1983), pp. 113-114

[9] Stiles, P.J., Kagan, M., Thermoconvective Instability of a Horizontal Layer of Ferrofuid in a Strong Magnetic Field, *J. Magn. Magn. Mater*., *85* (1990), pp.196-198

[10] Rudraiah, N., Sekhar, G.N., Convection in Magnetic Fluids with Internal Heat Source, *ASME. J. Heat Transfer, 113* (1991), pp. 122-127

[11] Recktenwald, A., Lücke, M., Thermoconvection in Magnetized Ferrofluids: the Influence of Boundaries with Finite Heat Conductivity, *J. Magn. Magn. Mater*., *188* (1998), pp. 326-332

[12] Shliomis, M.I., Smorodin, B.I. , Convection Instability of Magnetized Ferrofluids, *J. Magn. Magn. Mater., 252* (2002), 1-3, pp. 197-202

[13] Bozhko, A.A., Putin, G.F., Magnetic Action on Convection and Heat Transfer in Ferrofluid, *Indian. J. Eng. Mater. Sci*., *11* (2004), pp.309-314

[14] Odenbach, S., Völker, T., Thermal Convection in a Ferrofluid Supported by Therrmodiffusion, *J. Magn. Magn. Mater*., *289* (2005), pp.122-125

[15] Nanjundappa, C.E., Effect of MFD Viscosity on the Onset of Ferromagnetic Fluid Layer Heated from Below and Cooled from Above with Constant Heat Flux, *Measurm. Sci. Rev.*, *9* (2009), 3, pp.75-80

[16] Aggarwal, A.K., Makhija, S., Hall Effect on Thermal Stability of Ferromagnetic Fluid in Porous Medium in the Presence of Horizontal Magnetic Field, *Therm. Sci*., *18* (Supp.2) (2014), pp. S503-S514

[17] Yamaguchi, H., *et al*., Natural Convection in a Rectangular Box, *J. Magn. Magn. Mater*., *201* (1999), 1-3, pp.264-267

[18] Krakov, M.S., Nikiforov, I.V., To the Influence of Uniform Magnetic Field on Thermomagnetic Convection in Square Cavity, *J. Magn. Magn. Mater.*, *252* (2002), 1-3, pp. 209-221

[19] Krakov, M.S. *et al*., Three-dimensional Thermomagnetic Convection in a Cubic Cavity in the Presence of an External Uniform Magnetic Field, Magnetohydrodynamics, *40* (2004), 3, pp. 285-296

[20] Wen, C.Y., *et al*., Flow Visualization of Natural Convection of Magnetic Fluid in a Rectangular Hele-Shaw Cell, *J. Magn. Magn. Mater.*, *252* (2002), 1-3, pp. 206-208

[21] Wen, C.Y. , Su, W.P., Natural Convection of Magnetic Fluid in a Rectangular Hele-Shaw cell, *J. Magn. Magn. Mater*., *289* (2005), pp. 299-302

[22] Krakov , M.S., *et al*., Influence of the Uniform Magnetic Field on Natural Convection in Cubic Enclosure: Experiment and

Numerical Simulation, *J. Magn. Magn. Mater.*, *289* (2005), pp. 272-274
[23] Yamaguchi, H., *et al*., Thermomagnetic Natural Convection of Thermo-Sensitive Magnetic Fluids in Cubic Cavity with Heat Generating Object inside, *J. Magn. Magn. Mater*., *322* (2010), pp. 698-704
[24] Berkovsky, B.M. *et al*., Heat Transfer across Vertical Ferrofluid Layers, *Int. J. Heat Mass Transfer*, *19* (1976), pp. 981-986
[25] Kikura, H., *et al*., Natural Convection of a Magnetic Fluid in a Cubic Enclosure, *J.Magn.Magn.Mater*., *122* (1993), pp.315-318
[26] Sawada, T., *et al*., Visualization of Wall Temperature Distribution caused by Natural Convection of Magnetic Fluids in a Cubic Enclosure, *Int. J. Appl. Electromagn.Mater*., *4* (1994), pp. 329-335
[27] Bouhrour, A., Kalache, D., Natural Convection in a Ferroliquid, *Book of abstracts*, 9th International Conference on Magnetic Fluids, Bremen, Germany, 2001
[28] Snyder, S. M., *et al*., Finite Element Model of Magnetoconvection of a Ferrofluid, *J. Magn. Magn. Mater*., *262* (2003), pp. 269-279
[29] Ganguly, R., *et al*., Thermomagnetic Convection in a Square Enclosure using a Line Dipole, *Phys. Fluids*, *16* (2004), 7, pp. 2228-2236
[30] Jue, T.C., Analysis of Combined Thermal and Magnetic Convection Ferrofluid Flow in a Cavity, *Int. Commun. Heat and Mass Transfer*, *33* (2006), pp. 846-852
[31] Zablockis, D., *et al*., Numerical Investigation of Thermomagnetic Convection in Heated Cylindrical under the Magnetic Field of a Solenoid, *J. Phys. Condens. Matter., 20* (2008), pp. 301-308
[32] Contijo, R.G., Cunha, F.R., Experimental Investigation of Thermomagnetic Convection inside Cavities, *J. Nanosci. Nanotec., 12* (2012), 12, pp. 9198-9207
[33] Neuringer, J.L., Rosenweig, R.E., Ferrohydrodynamics, *Phys. Fluids*, *7* (1964), 12, pp. 1927-1937
[34] Rosenweig, R.E., *et al*., Viscosity of Magnetic Fluid in a Magnetic Field, *J. Colloid. Interf. Sci*., *29* (1969), 4, pp. 680-686
[35] Rosenweig, R.E., Magnetic Fluids, in: *Ferrohydrodynamics*, Cambridge University Press, 1985, pp. 33-73
[36] Bashtovoi, V.G., *et al*., Thermomechanics Equations for Magnetic Fluids7 of Equilibrium Magnetization, in: *Introduction to Thermomechanics of Magnetic Fluids*, Berkovsky (Ed.), NY, 1988, pp. 17-42
[37] Parekh, K., *et al*., Magnetocaloric Effect in Temperature Sensitive Magnetic Fluids, *Bul.Mater.Sci*., *23* (2000), pp.91-95
[38] Li, Q., *et al*., Investigation on Operational Characteristics of Miniature Automatic Cooling Device, *Int. J. Heat Mass Transfer*, *51* (2008), pp. 5033-5038
[39] Sustov, A.S., Thermomagnetic Convection in a Vertical Layer of Ferromagnetic Fluid, *Phys. Fluids*, *20* (2008), pp.1-18
[40] Engler, H., et al., Hindrance of Thermomagnetic Convection by the Magnetoviscous Effect, *Int. J. Heat Mass Transfer, 60* (2013), pp. 499-504
[41] Jordan, P.C., Association Phenomena in a Ferromagnetic Colloid, *Molecular Physics*, *25* (1973), 4, pp. 961-973
[42] Shliomis, M.I., Raikher, Y.L., Experimental Investigation on Magnetic Fluids, *IEEE Transactions on Magnetics*, *16* (1980), 2, pp. 237-250.
[43] McTague, J.P., Magnetoviscous Effect in Magnetic Colloids, *J. Chem. Physics, 51* (1969), pp.133-136
[44] Hamedani, H.M., Davis, L.R., An experimental Investigation of the Properties of Magnetic Fluid in Thermal Rejection Applications, *Proceeding of* Intersociety Energy Conversion Engineering Conference, New York, 1988, pp.359-364
[45] Li, Q., *et al.*, Experimental Investigation on Transport Properties of Magnetic Fluids, *Exp. Ther. Fluids. Sci., 30* (2002), pp.109-116
[46] De Risi, A., *et al*., High Efficiency Nanofluid Cooling System for Wind Turbines, *Therm. Sci.*, *18* (2014), 2, pp.543-554
[47] Kronkains, G., Measurement of Thermal and Electrical Conductivities of a Ferrifluid in a Magnetic Field, *Magnitnaya Gidrodinamica*, 3 (1977), pp. 138-140
[48] Philip, J., *et al.*, Evidence of Enhanced Thermal Conductivity through Percolating Structures in Nanofluids, *Nanotechnology, 19* (2008), 305706
[49] Nukirikiyimfura, I., *et al*., Effect of Chain-like Magnetite Nanoparticle Aggregates on Thermal Conductivity of Magnetic Nanofluid in Magnetic Field, *Exp. Therm. Fluid Sci*., *44* (2013), pp. 607-612,
[50] Fu, H.L., Gao, L., Theory for Anisotropic Thermal Conductivity of Magnetic Nanofluids, *Phys. Letters A*, *375* (2011), pp. 3588-3592
[51] Krichler, M., Odenbach, S., Thermal Conductivity Measurements on Ferrofluids with Special Reference to Measuring Arrangement, *J. Magn. Magn. Mater*., *326* (2013), pp. 85-90.
[52] Blums, E., Heat and Mass Transfer phenomena, *J. Magn. Magn. Mater.*, *252* (2002), 1-3, pp.189-193
[53] Bahiraei, M., Hangi, M., Flow and Heat Transfer Characteristics of a Magnetic Nanofluids: A review, *J. Magn. Magn. Mater*., *374* (2015), pp. 125-138
[54] Patankar, S.V., Numerical Heat Transfer and Fluid Flow, Hemisphere, Washington D.C. USA, 1980
[55] Davis, G. D.V., Natural Convection of Air in Square Cavity: a Benchmark Numerical Solution, *Int. J. Num. Methods Fluids*, *3* (1983), pp. 249-269
[56] Odenbach, S., Micrograyity Experiments on Thermomagnetic Convection in Magnetic Fluid, *J. Magn. Magn. Mater., 149* (1995), pp. 55-157
[57] Lankhorst, A.M., Laminar and Turbulent Natural Convection in Cavities. Numerical Modeling and Experimental Validation, Ph.D. Thesis, Technical University, Delt, 1991
[58] Sawada, T., *et al*., Natural Convection of a Magnetic Fluid in Concentric Horizontal Annuli in Non uniform Magnetic Fields, *Exp. Therm. Fluid. Sci*., *7* (1993), pp.212-220
[59] Chase, M.W. Jr. *et al.*, JANAF Thermochemical Tables, *J. Phys. Chem. Ref. Data*, *14* (1985), p.1203
[60] Kamiyama, S., *et al.*, On the Flow of a Ferromagnetic Fluid in a Circular Pipe, *Bull. JSME, 22* (1979), pp.1205-1211
[61] Poplewell, J., Al-Quenai, A., Thermal Conductivity Measurements on Ferofluids Containing Cobalt and Iron Particles, *J. Magn. Magn. Mater*., *65* (1987), pp.215-218
[62] Touloukian, Y.S., *et al.*, Thermophysical Properties of Matter, Plenum Press, New York, 1970, Vol.2, pp.154-156